

# Strategies for Shimming the Breast

Nimrod Maril,<sup>1</sup> Christopher M. Collins,<sup>2</sup> Robert L. Greenman,<sup>1</sup> and Robert E. Lenkinski<sup>1\*</sup>

**There is evidence in the literature indicating a significant static field inhomogeneity in the human breast. A nonhomogeneous field results in line broadening and frequency shifts in MRS and can cause intensity loss and spatial errors in MRI. Thus, there is a clear rationale for determining the regional variations in the static field homogeneity in the breast and providing strategies to correct them. Herein, the nature and extent of the static magnetic field at 3 T were measured in central planes of the human breast using both phase maps and multivoxel MRS techniques. In addition, the effect of first- and high-order shimming and of spatial saturation pulses on the static field inhomogeneity was evaluated. Both the theoretical and the measured field were found to be primarily linear in nature, with a reduction of 300 Hz from the nipple to the chest wall. First-order shimming reduced this inhomogeneity by 65%. Interestingly, the combination of spatial saturation pulses and first-order shimming was more effective than high-order shim alone. Since many clinical scanners do not have either higher-order shim or automated higher shimming algorithms that work in the presence of fat, the suggested combination provides an effective means to correct inhomogeneities in the breast. Magn Reson Med 54:1139–1145, 2005. © 2005 Wiley-Liss, Inc.**

**Key words:** breast; field homogeneity; phase map; CSI; high field

There is increasing interest in applying MRI and MRS of the breast for the detection and characterization of breast lesions. The rapid adoption of clinical whole-body MRI scanners, operating at higher field (3–4 T), provides the potential for improving the signal-to-noise ratio (SNR) of both MRI and MRS (1), provided that the field inhomogeneity can be “shimmed” out. Theoretically, the improvement in SNR is expected to be linear with the field (2). However, a comparison of proton spectra acquired from the human brain at 1.5 and 3 T showed a much lower improvement (1,3). Li et al. (1) suggested that this was probably due to a larger contribution of regional inhomogeneity at the higher field. These distortions in the static field result in line broadening and frequency shifts in MRS and can cause intensity loss and spatial errors in MRI.

A review of the literature describing the use of choline to characterize breast malignancy indicates that even at 1.5 T there maybe a significant contribution of field inhomogeneity to the line width of choline. Bakken et al. reported a

$T_2$  for choline of 320–360 ms in two breast cancer patients (4). A  $T_2$  of 320 ms corresponds to a line width of about 1 Hz. However, the experimental line widths of choline were as high as 8 Hz (5–10). At 4 T, Bolan et al. reported a  $T_2$  for choline of  $399 \pm 133$  ms (11). These authors fit the choline peak to a voigt line shape with a Lorentzian line width of 0 Hz and a Gaussian line of 14 Hz. These results indicate that there may be a significant contribution of  $T_2^*$  to the line width of choline, and thus, it may be possible to gain a significant increase in SNR by reducing the contribution of static field inhomogeneity.

A nonhomogeneous static field also affects the performance of echo-planar imaging (12), chemically selective fat suppression, and the successful suppression of water in localized MRS (13,14). Although the fat/water separation can be achieved in the breast even in the presence of a nonhomogeneous field using the three-point Dixon method (15), the application of selective spectral and spatial excitation pulses (16,17) is efficient only in the presence of a relatively homogeneous field. These considerations suggest that there is a clear rationale for determining the regional variations in field homogeneity in the breast and providing strategies to correct them.

The static magnetic field in the brain has been measured in vivo by various techniques [(18) and references cited therein (19)]. A three-dimensional model of the magnetic field variation in the human brain was recently calculated taking into account the shape of the head and the magnetic susceptibility of the tissues: bone, soft tissue, and air (20). While the shape of the brain is almost spherical, the shape and tissue composition of the breast will vary among subjects. Consequently, the patterns of field inhomogeneity in the breast might be expected to vary from subject to subject more than those in the brain.

The aim of this study was to evaluate, for the first time, the nature and the extent of the static magnetic field in the human breast. The field was measured using both phase maps (15,21) and multivoxel MRS. Although the latter is very slow (17 min), it was less vulnerable to imperfections in the pulse sequence and to reconstruction issues than the phase map method. Therefore, the CSI method in this study served as a gold standard. The experimental results were compared with those obtained from a mathematical model of the field in a representative breast (20). Both the theoretical and the measured field were primarily linear in nature with relative strong nonlinear components near the nipple and the chest wall. Interestingly, the field patterns were dependent on the shape of the breast and the position of the nipple.

## METHODS

### Field Modeling

A three-dimensional model of a healthy human breast was created by manually segmenting MRI data from a normal

<sup>1</sup>Department of Radiology, Beth Israel Deaconess Medical Center, Harvard Medical School, Boston, Massachusetts, USA.

<sup>2</sup>Department of Radiology, Pennsylvania State University College of Medicine, Hershey, Pennsylvania, USA.

Grant Sponsor: National Institutes of Health (NIH); Grant Number CA098389.

\*Correspondence to: Robert E. Lenkinski, Director, MRI Research, Beth Israel Deaconess Medical Center, 330 Brookline Avenue, AN-224, Boston, MA 02215, USA. E-mail: rlenkins@bidmc.harvard.edu

Received 4 March 2005; revised 15 June 2005; accepted 5 July 2005.

DOI 10.1002/mrm.20679

Published online 10 October 2005 in Wiley InterScience (www.interscience.wiley.com).

volunteer ( $T_1$ -weighted, multislice, 16 cm FOV,  $256 \times 256$  matrix, and slice thickness of 1 cm) into bone, lung, soft tissue, and air. These regions were then assigned relative magnetic susceptibilities of 0.99998869, 0.99999568, 0.99999096 (22), and 1.0000004 (23), respectively. The value for lung was obtained by taking the average of the values for soft tissue and air. The ends of the model were extended to move artificial air—tissue interfaces far from the region of interest. A previously published method was then used to find the magnetic field distribution in the model (20).

### Volunteers

Seven female volunteers (age range, 21–32 years; mean age,  $24 \pm 7$  years [mean  $\pm$  SD]) were enrolled in this study. Informed consent was obtained in accordance with the guidelines of the Institutional Review Board of the Beth Israel Deaconess Medical Center.

### MRI

The studies were performed using a 3 T scanner (Signa LX, General Electric, Waukesha, WI, USA) equipped with a body coil (length 53 cm, diameter 55 cm) for RF transmission and a four-element breast phased-array coil for receiving, two coils for each breast. The region for MRS was selected graphically from a sagittal,  $T_2$ -weighted, spin echo image (TE/TR of 4000/35 ms), acquired using a FOV of  $16 \times 16$  cm<sup>2</sup>, matrix size of  $256 \times 256$ , and slice thickness of 1 cm. Images and CSI data sets were acquired before and after a first-order shim was applied on the FOV.

### Phase Maps

The measurement of the  $B_0$  field distribution was achieved from phase maps that were constructed from images that were recorded using a spin-echo pulse sequence that was developed to allow changes to be introduced in the timing between the RF excitation and refocusing pulses. Images of the central sagittal slice of the breast were acquired using a FOV of  $16 \times 16$  cm<sup>2</sup> and  $32 \times 32$  matrix size, with TE/TR of 68/600 ms during a single breath hold (21 s). Axial images of the bilateral breasts were acquired in a similar manner using a FOV of  $40 \times 40$  cm<sup>2</sup> and  $256 \times 256$  matrix size (2.32 min). The RF frequency was set to the water resonance during the calibration process. First, an image was acquired where the spacing between the excitation pulse and the refocusing pulse was equal to one half that of the echo formation time (23 ms) at the center of the readout gradient. This resulted in an image in which the lipid and water signals were in phase. A second image was then acquired with the time of the refocusing pulse shifted by 2.35 ms with respect to both the excitation pulse and the center of the readout gradient. Thus, in the second image the lipid and water signals are both at a phase shift of  $2\pi$  radians relative to their phase in the first image. Unwrapping  $2\pi$  jumps in the phase map images was achieved by an algorithm that was based on the 2D region growing approach, described previously (15), using a locally developed IDL (Research System, Inc., Boulder, CO, USA) program. After the phases in each of the phase maps were unwrapped, the phase map of the first image was sub-

tracted from that of the second. The field at each spatial location ( $\Delta B_{ij}$ ) was calculated according to the equation

$$\Delta B_{ij} = \frac{\Delta\phi_{ij}}{\gamma \times \Delta t}$$

where  $\Delta\phi$  is the difference in the phase between the first and the second image, and  $\Delta t$  is the shifted time of the refocusing pulse.

### CSI

Multivoxel MRS data sets were recorded with PRESS selection (typically  $10 \times 10$  cm<sup>2</sup>) and two-dimensional (2D) phase encoding, with a TR/TE of 1000/35 ms. The <sup>1</sup>H multivoxel spectroscopy data were acquired without using water suppression in 15 min as a  $32 \times 32$  matrix with a FOV of  $16 \times 16$  cm<sup>2</sup> and a slice thickness of 1 cm (0.25 cm<sup>3</sup> voxel volume), using 512 time points and a spectral width of 2500 Hz. After acquisition, the spectral data from each receiver were transferred to a SPARC workstation (Sun Microsystems, Mountain View, CA, USA) and initially processed using Sage/IDL. This initial processing included line broadening of 10 Hz, zero filling of the spectral domain, 3D Fourier transformation, and phasing. Then the data were further analyzed using a locally developed IDL program. The program searched the water and the lipid resonances at each spatial location. These frequencies were found by looking at the maximum of the peak between 3.5 to 6 ppm and 0.5 to 2.5, respectively. The field map (in Hertz) was calibrated by subtracting 600 Hz (4.7 ppm at 3 T) from the calculated frequency of water at each spatial location.

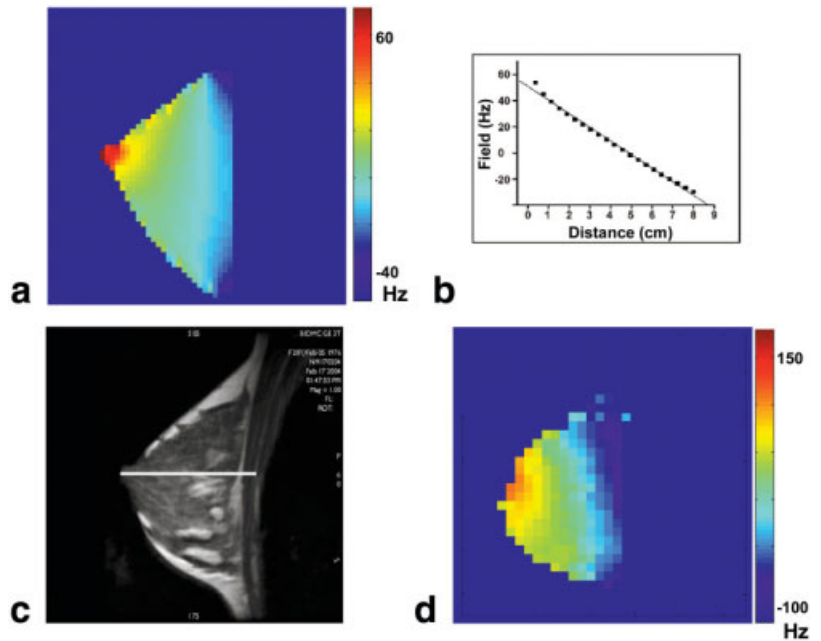
### Shim simulation

The effects of both linear and high-order shimming were simulated by sequentially fitting the measured field to surfaces that represent the corresponding shim operations and then by subtracting the fitted surface from the field. The residual was used for fitting the next “shim” surface. Since the field was measured along a sagittal or an axial plane, the first-order shim was simulated by fitting the field to  $Z$  and  $Y$  or  $X$  and  $Y$ , respectively. For the same reason only the relevant surfaces were used to simulate the high-order shim. For example, in the sagittal the planes representing  $Z^2$ ,  $Y^2$ ,  $Z^2$ ,  $ZY$ ,  $Z^3$ ,  $Y^3$ , and  $Z^2-Y^2$  were used. Spatial saturated pulses were simulated by graphic prescription, omitting peripheral parts of the breast from the image, especially the nipple area and the chest wall corresponding to the eight possible spatial saturation pulses that exist in our scanner prior to the shim simulation. The homogeneity was assessed by taking the SD of the field distribution. Statistical analysis to evaluate differences between shimming strategies was performed by means of a two-tailed paired Student’s  $t$  test. Results are presented as means  $\pm$  standard error of the mean (SEM).

## RESULTS

A simulation of the  $B_0$  field in the sagittal plane of the breast is shown in Fig. 1a. The field was calculated as

FIG. 1. (a)  $B_0$  map calculated from a model of the individual breast in the sagittal plane as described under Methods. The field was calculated from the  $T_2$ -weighted MR image shown in c by assigning the relative magnetic field susceptibilities to the different tissue compartments in the breast as described under Methods. According to the model, the field decreases from the nipple to the chest wall. (b) A profile of the calculated  $B_0$  field from the nipple to the chest wall along the white line marked on c. (d) Measurement of the  $B_0$  field, in the same plane shown in c, by the multivoxel MRS method yielded a similar pattern as in the calculated field.



described under Methods by taking into account the shape of the breast shown in Fig. 1c and the susceptibility differences between its various compartments (fat, water, air, etc.). According to this model, the variation in the static magnetic field inhomogeneity in the breast is over  $\sim 140$  Hz for a 3 T magnet. The SD of the field distribution was 29 Hz. Moreover, the field decreases in a linear manner from the nipple to the chest wall (Fig. 1b). Also, the model shows that there are regions of high gradients of the

static field near the nipple. Simulation of first- and high-order shim operations reduced the inhomogeneity to 11 and 9 Hz, respectively. As expected, the combination of applying spatial saturation pulses to remove the effects of the regions of high gradients of the static field and high-order shims was the most effective way to reduce field inhomogeneity (5 Hz). Interestingly, the simulation showed that the combination of spatial saturation pulses and first-order shim (6 Hz) reduced field inhomogeneity

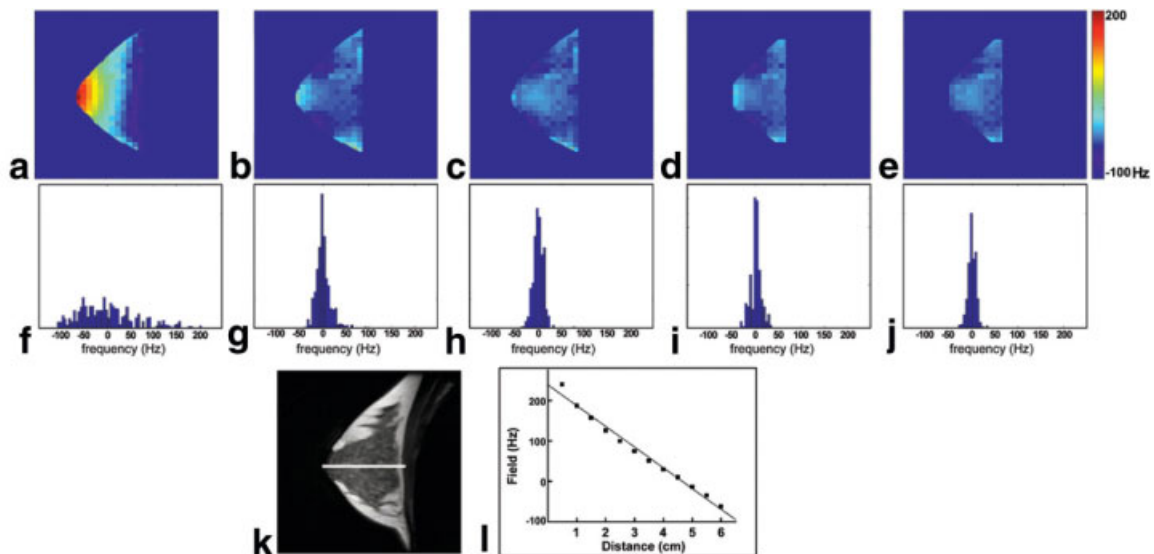


FIG. 2. (a) A typical field map of a normal volunteer individual breast in the sagittal plane measured by the phase map technique. (b) A field map of the same plane measured after applying first-order shim. (c–e) Simulations of the effects of high-order shim, first-order shim + spatial saturation pulses, and high-order shim + spatial saturation pulses, respectively, on the homogeneity of the field shown in a. The simulations were performed by fitting the calculated field to surfaces that represent the corresponding shim operation as described under Methods and by subtracting the fitted surface from the original field. (f–j) The frequency distributions over the breast calculated from the field maps of a–e, respectively, showing the improvement of field homogeneity after applying the corresponding shim operations. (k) A  $T_1$ -weighted image of the same sagittal plane of the breast of a normal volunteer from which the field shown in a was measured. (l) A profile of the calculated  $B_0$  field from the nipple to the chest wall along the white line marked on k.

Table 1  
The Standard Deviations of the Static Field in the Central Plane of the Breast at 3T under the Conditions Described

Shim type	Field inhomogeneity (Hz)
No shim (sag) <sup>a</sup>	58.1 ± 4.0
No shim (ax one breast) <sup>b</sup>	59.2 ± 2.1
Manual first-order shim (ax one breast) <sup>b</sup>	21.4 ± 2.0
First-order shim (sag) <sup>a</sup>	20.0 ± 2.0
High-order shim simulation (sag) <sup>a</sup>	14.6 ± 0.8
First-order shim+saturation pulses (sag) <sup>a</sup>	13.6 ± 1.6
High-order shim+saturation pulses (sag) <sup>a</sup>	9.8 ± 2.0

Note. sag, sagittal plane; ax, axial plane.

<sup>a</sup> $n = 7$ .

<sup>b</sup> $n = 5$ .

more effectively than applying high-order shims alone. Measurement of the static magnetic field of the same sagittal plane used for the simulation, from multivoxel MRS (Fig. 1d), yielded a decrease in the field from the nipple to the chest wall in the same manner as that which appeared in the theoretical model.

The multivoxel MRS technique was limited to areas of the breast that contained water. Therefore, we have measured the field by the phase map method, which is fast and covers the whole breast. In order to verify the accuracy of the measurement of the field from the phase maps, the field was also measured independently by the multivoxel MRS technique. As expected, in all of the cases ( $n = 10$ ) the static field measured with the phase map technique was identical to that measured with the multivoxel MRS technique indicating the accuracy of the measurements.

The extent of field inhomogeneity over the whole breast in the sagittal plane was more than twice as high ( $58 \pm 4$  Hz,  $n = 7$ ) as that found by the theoretical model (Fig. 2 and Table 1). This finding was probably due to the initial shim setting of the magnet. The linear component of the field inhomogeneity from the nipple to the chest wall was almost completely eliminated by applying a first-order shim (Fig. 2b). As a result, the field inhomogeneity over the breast was reduced to  $20 \pm 2$  Hz. Simulation of the linear shim yielded a similar effect on field homogeneity, which indicated the efficiency of the first-order shim of the scanner. The percentage of the linear component of the static field inhomogeneity of the total field inhomogeneity ( $65 \pm 7\%$ ) is almost identical to that in the calculated model (62%). According to our simulation, applying a linear shim and spatial saturation pulses reduced the field inhomogeneity to  $13.6 \pm 1.6$  Hz. This did not have a significantly different effect on the field homogeneity ( $P > 0.05$ ) than applying high-order shims over the whole breast (Table 1). As predicted by the mathematical model, the field in the breast was significantly more homogenous ( $9.8 \pm 2.0$  Hz,  $P < 0.01$ .) when the combination of high-order shims and spatial saturation pulses was applied than when the other methods were applied (Table 1).

Figure 3 demonstrates the field distribution in a typical large breast that touched the coil, consequently distorting the shape of the breast. The model predicted that the pattern of the field is determined primarily by the shape of

the breast and not by the internal distribution of the tissue compartments. Indeed, the pattern of the field in these breasts ( $n = 3$ ) was not similar to that in the other cases where the breast maintained its half-sphere shape ( $n = 7$ ). Note that the range of the field in the distorted breast is much higher than that in the nondistorted one (Fig. 2). In addition, since the pattern of the field was not linear, a first-order shim was not as efficient as in the half-sphere-like breasts (Fig. 3c).

Investigation of the static magnetic field in the axial plane revealed that each breast exhibited the same field pattern that was observed in the sagittal plane (Fig. 4a). This pattern included a dominant linear gradient along the anterior–posterior axis and a nonlinear variation along the left–right axis (Fig. 4b and c). The field gradient along the anterior–posterior axis was dominant even when the static field was measured in both breasts (Fig. 4b and c). Interestingly, the automated first-order shim algorithm provided by GE could not eliminate the linear components of the field distribution, and as a result, the field measured after automated first-order shimming was very similar to that measured before shimming. These linear components could be eliminated by a manual first-order shim (Fig. 4d). This elimination reduced the field variation by 60%, which was similar to the findings in the sagittal plane (Table 1).

## DISCUSSION

In their calculation of the static field in the brain, Collins et al. (20) predicted about a 0.3-ppm difference in field associated primarily with the differences in susceptibilities between gray and white matter in axial slices above the ventricles. This would correspond to about a 40-Hz difference in the static field at 3 T. In the breast where the variation in size (and presumably shape) and tissue composition is greater than in the brain, we should expect a more complex field pattern with greater variation between individuals. The volume of the human breast has been reported (25) to range from about 150 to 2300 mL. Also, the percentage of glandular tissue in the breast has been shown to be variable, particularly with the age of the woman (43–50%) and the size of the breast (31–80%) (26).

The calculation of the field in the breast showed a predominantly linear decrease in the field along the anterior–posterior axis. We suggest that this pattern is primarily determined by the shape of the breast and the position of the nipple. The calculation clearly shows that the nipple creates a local region of high static field within the breast. Our experimental results are in agreement with these calculations. The precise shape of the breast probably influences the slope of the linear field variation in each individual patient. The correction of this linear gradient with linear shims reduces the variations in the static field by about 65% within the breast. We suggest that the remaining differences in field homogeneity reflect both variations in the tissue composition of the breast (glandular versus fat) and their spatial distributions.

The differences in tissue composition in the breast place an additional constraint on the methods used to create field maps. Since the glandular tissues contain primarily water and little fat and the fat tissues show the reverse, the

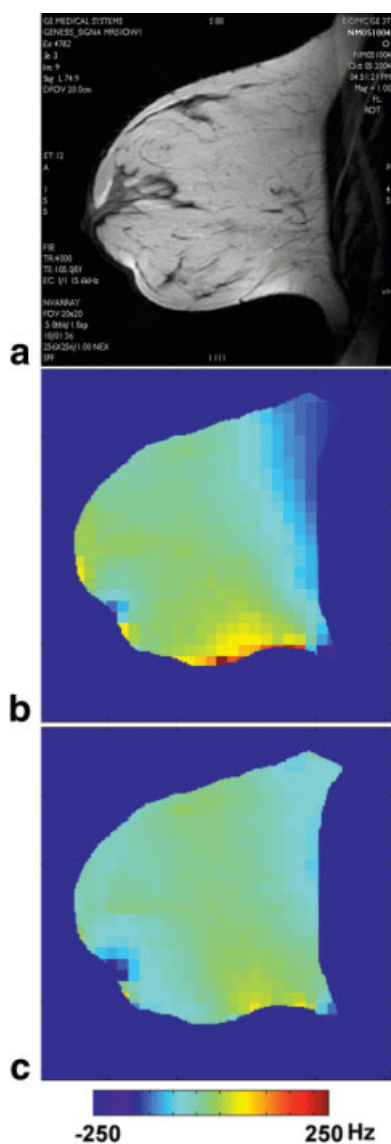


FIG. 3. The effect of the shape of the breast on field distribution. (a)  $T_1$ -weighted image of a typical large breast where its shape was distorted by the coil. (b and c) Field maps of the same breast shown in a, before and after first-order shim, respectively. Note the focal areas of field inhomogeneities where the half-sphere shape of the breast is distorted.

use of only the water resonance in either phase mapping sequences or MRS CSI methods may lead to incomplete field maps. In principle, the field could be mapped over the whole breast using the CSI method by integrating the two maps, a map of the glandular area using the water resonance and a map of the fat area using the lipid resonance. However, this method is time consuming. For example, mapping the field in the axial plane over the two breasts with an in-plane resolution similar to that used for mapping the field in the individual breast (in plane resolution of  $\sim 0.25 \text{ cm}^2$ ) would require  $\sim 3 \text{ h}$ . Consequently, although the MRS method is minimally subjected to errors, it cannot be applied in clinical protocols. In contrast, the acquisition time of the phase map method is very short, and the map covers the whole breast regardless of

the fat and glandular distributions. Accordingly, we employed a phase mapping method where both fat and water were in phase, using a homebuilt phase unwrapped algorithm that was based on the region growing approach (15). It should be noted, however, that the phase map method is vulnerable to imperfections in the pulse sequence, such as the timing between the RF excitation and refocusing. Therefore, the additional measurement of the field with the independent multivoxel MRS method served to verify the accuracy of the field measurement with phase map method.

The results presented here indicate that the best overall field homogeneity in the breast was achieved when high-order shims together with spatial presaturation of the nipple and chest wall were applied. This reduces the static field from about 60 Hz to about 10 Hz. In a clinical scanner, automated high-order shim is being performed using a region of interest (ROI). This is done in order to achieve very high field homogeneity within the ROI while neglecting, and potentially degrading, the homogeneity outside the ROI. The spatial saturation pulses used in this study simulated also the ROI since it eliminated areas of high field inhomogeneity, such as the nipple and the chest wall. It is very interesting to note that the combination of linear shimming with spatial presaturation of the nipple and chest wall reduces the field variation from 60 to about 14 Hz, which is almost as good as the results obtained with higher-order shimming. The strategy of using the linear shimming approach with spatial presaturation may offer an attractive alternative since there may be MR systems that do not have either higher-order shims or automated higher shimming algorithms that work in the presence of fat. The suggested combination is not applicable in cases where the suspected lesion is near the nipple or the chest wall. For such cases and in the absence of an automated high-order shim, we suggest applying dynamic manual high-order shim where this option is possible by the scanner. Since the phase map algorithm is very fast, the improvement of the field homogeneity near the lesion can be measured after each step of shimming.

The fact that spatial presaturation of the nipple and chest wall has such a large improvement supports our earlier suggestion that the static field within the breast is primarily determined by the size and shape of the breast together with the position of the nipple. Indeed, in large breasts where their shape was distorted by the coil, the field was no longer linear and contained focal areas of strong field inhomogeneities, which could not be eliminated by first-order shim. These focal areas were at the edges of the breast and, therefore, may be eliminated by spatial saturation pulses. In addition, we suggest that it is of advantage to employ breast coils of different sizes to retain the half sphere shape of the breast while maintaining the filling factor.

Investigation of the field in both breasts in the axial plane revealed that each breast exhibits a similar field pattern to that observed in the sagittal plane, as would be expected from considerations of symmetry. The variation of the field over the two breasts along the left–right axis was smaller than that over the individual breast along the

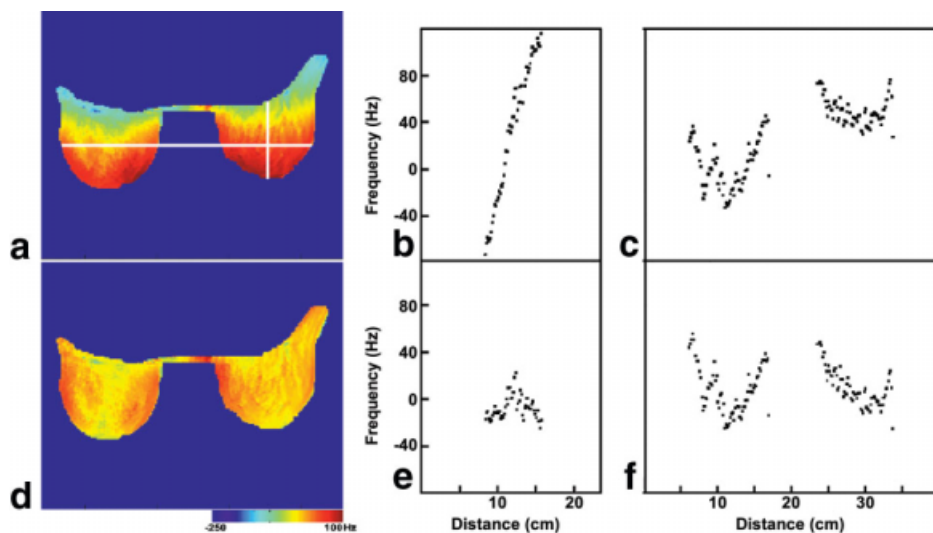


FIG. 4. Typical field maps of normal volunteer bilateral breasts in the axial plane measured by the phase map technique prior (a) and after (d) applying first-order shim. (b and c) Profiles of the field before shimming along the vertical and horizontal lines, respectively, marked on a. (e and f) Profiles of the field after shimming along the vertical and horizontal lines, respectively, marked on a.

anterior–posterior axis. This finding indicates again that the half-sphere-like shape of the breast affects the field more than all the other factors, such as the tissue compositions and the adjacent organs. Moreover, as the automated shimming procedure could not shim the FOV that included both breasts, we suggest scanning the individual breast when sequences requiring a homogeneous field are used. After linear shimming there are residual field patterns observed in each breast that may not be effectively shimmed using a single set of high-order shim values. This may result in incomplete fat suppression in bilateral axial studies of the breast acquired with a large FOV. This problem can be avoided by using an interleaved small FOV, axial single breast excitations with higher-order shim values set dynamically for each breast.

The static field was measured, in this study, over a single central axial or sagittal plane of the breast. A volumetric measurement of the field in the breast requires either a multislice or a 3D phase mapping method, which were not available in our scanner. Nevertheless, noncentral sagittal planes exhibited a pattern of field homogeneity similar to that in the central sagittal plane. Therefore, we can assume from the distribution of the field along the axial plane that the extent of the linear component of the field inhomogeneity in the whole half-sphere-like breast will be close to that in the central sagittal plane.

The reduction in the static field in the breast to about 10–14 Hz at 3 T means that it should be possible to achieve good water suppression across the breast. At 1.5 T the variation in field would be halved. The possibility of achieving effective water suppression is particularly important for multivoxel MRS studies like those reported by Jacobs et al. (27) at 1.5 T. Similar conclusions can be made for studies involving echo-planar imaging of the breast. Based on the results presented here, we suggest that the improvements in the static field in the breast, achievable using the strategies outlined in this paper, make the use of selective excitation methods based on spectrally selective RF pulses or spatial–spectral pulses feasible.

## REFERENCES

- Li BS, Regal J, Gonen O. SNR versus resolution in 3D  $^1\text{H}$  MRS of the human brain at high magnetic fields. *Magn Reson Med* 2001;46:1049–1053.
- Norris DG. High field human imaging. *J Magn Reson Imaging* 2003;18:519–529.
- Barker PB, Hearshen DO, Boska MD. Single-voxel proton MRS of the human brain at 1.5T and 3.0T. *Magn Reson Med* 2001;45:765–769.
- Bakken IJ, Gribbestad IS, Singstad TE, Kvistad KA. External standard method for the in vivo quantification of choline-containing compounds in breast tumors by proton MR spectroscopy at 1.5 Tesla. *Magn Reson Med* 2001;46:189–192.
- Cecil KM, Schnall MD, Siegelman ES, Lenkinski RE. The evaluation of human breast lesions with magnetic resonance imaging and proton magnetic resonance spectroscopy. *Breast Cancer Res Treat* 2001;68:45–54.
- Yeung DK, Cheung HS, Tse GM. Human breast lesions: characterization with contrast-enhanced in vivo proton MR spectroscopy—initial results. *Radiology* 2001;220:40–46.
- Roebuck JR, Cecil KM, Schnall MD, Lenkinski RE. Human breast lesions: characterization with proton MR spectroscopy. *Radiology* 1998;209:269–275.
- Kvistad KA, Bakken IJ, Gribbestad IS, Ehrnholt B, Lundgren S, Fjosne HE, Haraldseth O. Characterization of neoplastic and normal human breast tissues with in vivo ( $^1\text{H}$ ) MR spectroscopy. *J Magn Reson Imaging* 1999;10:159–164.
- Jagannathan NR, Kumar M, Seenu V, Coshic O, Dwivedi SN, Julka PK, Srivastava A, Rath GK. Evaluation of total choline from in-vivo volume localized proton MR spectroscopy and its response to neoadjuvant chemotherapy in locally advanced breast cancer. *Br J Cancer* 2001;84:1016–1022.
- Gribbestad IS, Singstad TE, Nilsen G, Fjosne HE, Engan T, Haugen OA, Rinck PA. In vivo  $^1\text{H}$  MRS of normal breast and breast tumors using a dedicated double breast coil. *J Magn Reson Imaging* 1998;8:1191–1197.
- Bolan PJ, Meisamy S, Baker EH, Lin J, Emory T, Nelson M, Everson LI, Yee D, Garwood M. In vivo quantification of choline compounds in the breast with  $^1\text{H}$  MR spectroscopy. *Magn Reson Med* 2003;50:1134–1143.
- Jezzard P, Balaban RS. Correction for geometric distortion in echo planar images from  $B_0$  field variations. *Magn Reson Med* 1995;34:65–73.
- Dixon WT. Simple proton spectroscopic imaging. *Radiology* 1984;153:189–194.
- Skinner TE, Glover GH. An extended two-point Dixon algorithm for calculating separate water, fat, and  $B_0$  images. *Magn Reson Med* 1997;37:628–630.
- Szumowski J, Coshow WR, Li F, Quinn SF. Phase unwrapping in the three-point Dixon method for fat suppression MR imaging. *Radiology* 1994;192:555–561.

16. Hardy PA, Recht MP, Piraino DW. Fat suppressed MRI of articular cartilage with a spatial-spectral excitation pulse. *J Magn Reson Imaging* 1998;8:1279–1287.
17. Zur Y. Design of improved spectral-spatial pulses for routine clinical use. *Magn Reson Med* 2000;43:410–420.
18. Li S, Dardzinski BJ, Collins CM, Yang QX, Smith MB. Three-dimensional mapping of the static magnetic field inside the human head. *Magn Reson Med* 1996;36:705–714.
19. Sutton BP, Noll DC, Fessler JA. Dynamic field map estimation using a spiral-in/spiral-out acquisition. *Magn Reson Med* 2004;51:1194–1204.
20. Collins CM, Yang B, Yang QX, Smith MB. Numerical calculations of the static magnetic field in three-dimensional multi-tissue models of the human head. *Magn Reson Imaging* 2002;20:413–424.
21. Wang Y, Li D, Haacke EM, Brown JJ. A three-point Dixon method for water and fat separation using 2D and 3D gradient-echo techniques. *J Magn Reson Imaging* 1998;8:703–710.
22. Hopkins JA, Wehrli FW. Magnetic susceptibility measurement of insoluble solids by NMR: magnetic susceptibility of bone. *Magn Reson Med* 1997;37:494–500.
23. Krauss J. *Electromagnetics*. New York: McGraw-Hill, 1984.
24. Katz-Brull R, Rofsky NM, Lenkinski RE. Breathhold abdominal and thoracic proton MR spectroscopy at 3T. *Magn Reson Med* 2003;50:461–467.
25. Kalbhen CL, McGill JJ, Fendley PM, Corrigan KW, Angelats J. Mammographic determination of breast volume: comparing different methods. *Am J Roentgenol* 1999;173:1643–1649.
26. Jamal N, Ng KH, McLean D, Looi LM, Moosa F. Mammographic breast glandularity in Malaysian women: data derived from radiography. *Am J Roentgenol* 2004;182:713–717.
27. Jacobs MA, Barker PB, Bottomley PA, Bhujwala Z, Bluemke DA. Proton magnetic resonance spectroscopic imaging of human breast cancer: a preliminary study. *J Magn Reson Imaging* 2004;19:68–75.